PAPER

Fabrication of MSC-laden composites of hyaluronic acid hydrogels reinforced with MEW scaffolds for cartilage repair

To cite this article: Jonathan H Galarraga *et al* 2022 *Biofabrication* **14** 014106

Biofabrication

PAPER

Fabrication of MSC-laden composites of hyaluronic acid hydrogels reinforced with MEW scaffolds for cartilage repair

Jonathan H Galarraga[1], Ryan C Locke[2,3], Claire E Witherel[1], Brendan D Stoeckl[1,2,3], Miguel Castilho[4,5], Robert L Mauck[1,2,3], Jos Malda[4,6], Riccardo Levato[4,6] and Jason A Burdick[1,*]

[1] Department of Bioengineering, University of Pennsylvania, Philadelphia, PA, United States of America
[2] Translational Musculoskeletal Research Center, Philadelphia VA Medical Center, Philadelphia, PA, United States of America
[3] Department of Orthopaedic Surgery, University of Pennsylvania, Philadelphia, PA, United States of America
[4] Department of Orthopaedics, University Medical Center—Utrecht, Utrecht, The Netherlands
[5] Department of Biomedical Engineering, Technical University of Eindhoven, Eindhoven, The Netherlands
[6] Department of Clinical Sciences, Utrecht University, Utrecht, The Netherlands
[*] Author to whom any correspondence should be addressed.

E-mail: burdick2@seas.upenn.edu

RECEIVED
15 September 2021

REVISED
10 November 2021

ACCEPTED FOR PUBLICATION
17 November 2021

PUBLISHED
1 December 2021

Keywords: melt-electrowriting, hydrogel, cartilage, interfacial strength, tissue integration

Supplementary material for this article is available online

Abstract

Hydrogels are of interest in cartilage tissue engineering due to their ability to support the encapsulation and chondrogenesis of mesenchymal stromal cells (MSCs). However, features such as hydrogel crosslink density, which can influence nutrient transport, nascent matrix distribution, and the stability of constructs during and after implantation must be considered in hydrogel design. Here, we first demonstrate that more loosely crosslinked (i.e. softer, ∼2 kPa) norbornene-modified hyaluronic acid (NorHA) hydrogels support enhanced cartilage formation and maturation when compared to more densely crosslinked (i.e. stiffer, ∼6–60 kPa) hydrogels, with a >100-fold increase in compressive modulus after 56 d of culture. While soft NorHA hydrogels mature into neocartilage suitable for the repair of articular cartilage, their initial moduli are too low for handling and they do not exhibit the requisite stability needed to withstand the loading environments of articulating joints. To address this, we reinforced NorHA hydrogels with polycaprolactone (PCL) microfibers produced via melt-electrowriting (MEW). Importantly, composites fabricated with MEW meshes of 400 μm spacing increased the moduli of soft NorHA hydrogels by ∼50-fold while preserving the chondrogenic potential of the hydrogels. There were minimal differences in chondrogenic gene expression and biochemical content (e.g. DNA, GAG, collagen) between hydrogels alone and composites, whereas the composites increased in compressive modulus to ∼350 kPa after 56 d of culture. Lastly, integration of composites with native tissue was assessed *ex vivo*; MSC-laden composites implanted after 28 d of pre-culture exhibited increased integration strengths and contact areas compared to acellular composites. This approach has great potential towards the design of cell-laden implants that possess both initial mechanical integrity and the ability to support neocartilage formation and integration for cartilage repair.

1. Introduction

Articular cartilage damage is a pervasive problem that significantly inhibits quality of life and joint mobility in afflicted patients [1]. Focal defects on the articulating surface of joints may form in patients due to trauma, sports injuries, or daily activities associated with joint function [2]. Native cartilage unfortunately does not possess significant regenerative capacity [3], and these defects may further progress if left untreated, resulting in significant pain and dysfunction [4]. To this end, a number of clinical approaches have been developed for cartilage defect repair, including microfracture, mosaicplasty, and

matrix-assisted chondrocyte implantation (MACI) [5]. However, despite their promise, these surgical procedures often result in repair cartilage with inferior composition and mechanical properties when compared to healthy hyaline cartilage [1, 6, 7]. Thus, there is a continued and significant clinical need for the development of new approaches that support the restoration of functional cartilage.

Hydrogels have emerged as a promising approach for the encapsulation of cells that then synthesize and organize nascent cartilagenous extracellular matrix (ECM). A range of materials have been used for the formation of neocartilage from cell-laden hydrogels [8], and advancements in both hydrogel processing and our ability to incorporate physiochemical cues within hydrogels (e.g. patterning of singaling ligands, controlled release of biochemical signals) have improved the quality of engineered cartilage *in vitro* [9]. Towards translating these hydrogels into the clinic, biofabrication approaches have enabled the fabrication of cell-laden hydrogels with patient-specific geometries and high porosity. For instance, the biopen is a handheld device that permits extrusion of bioinks into focal cartilage defects intraoperatively, such that cartilage repair can occur *in situ* within defects [10, 11]. Other extrusion-based bioprinting techniques have facilitated the expansion of candidate bioinks for cartilage tissue engineering [12], while lithographic and new tomographic bioprinting approaches have drastically improved the resolution and throughput with which cell-laden implants can be engineered [13, 14]. Despite these recent advances in bioprinting, one of the persistent challenges associated with engineering hydrogels for cartilage tissue engineering is the balance of two, opposing design criteria. Specifically, hydrogels with large mesh sizes are promising candidates given their ability to maintain cell viability and to promote the distribution of deposited matrix, but these hydrogels have much lower initial mechanical properties [15, 16].

Hydrogels with tunable degradability have been engineered to address this challenge, such that higher initial mechanical properties can be achieved while cell-mediated enzymatic degradation ensures that the mesh size increases over time, permitting matrix distribution and cartilage maturation [17]. Similarly, hydrolytically degradable polyethylene glycol (PEG) and hyaluronic acid (HA) hydrogels were designed to improve matrix production and distribution by encapsulated chondrocytes and mesenchymal stromal cells (MSCs), respectively, when compared to non-degradable hydrogel controls [18, 19]. However, these approaches are generally still limited with regards to initial hydrogel mechanics due to cell viability concerns, and they also require that the rate of hydrogel degradation be carefully balanced with the rate of tissue formation and maturation to maintain mechanical properties [20].

Alternatively, a range of strategies have been employed to enhance the mechanical properties of hydrogels for cartilage repair. Interpenetrating network (IPN) hydrogels, which are composed of multiple interdigitating networks, are one approach to engineer hydrogels with high toughness. By tuning the properties of combined brittle and ductile networks at the molecular scale, non-additive increases in hydrogel moduli can be achieved [21]. As an alternative, extruded polycaprolactone (PCL) may be incorporated within 3D printed hydrogels (e.g. fibrin-collagen, alginate, agarose, PEG) containing encapsulated chondrocytes or MSCs for cartilage formation [22–26]. PCL is a well-established biomaterial with extended degradation profiles and significantly higher moduli than traditional hydrogels, such that its combination with hydrogels results in improved mechanical integrity. To this end, electrospun nanofibrous PCL scaffolds have been incorporated into bioprinted hydrogels to improve both the shape fidelity and mechanical properties of fabricated constructs [27]. In another approach, IPNs composed of alginate and methacryloyl-modified gelatin (GelMA) were reinforced with 3D printed PCL templates towards recapitulating the tension-compression non-linearity of native cartilage [28, 29]. A multi-head printing setup enabled fabrication of these composites with encapsulated MSCs and chondrocytes toward the formation of hyaline cartilage [28]. However, while IPNs or composite scaffolds containing PCL may improve the mechanical properties of cell-laden hydrogels, these approaches can also reduce the relative volume available for the formation of new tissue by embedded cells [30].

In response to this design limitation, reinforcement of printed GelMA hydrogels with PCL microfibers has been achieved via melt-electrowriting (MEW) [31, 32]. MEW is a biofabrication process that allows for the controlled deposition of electrically charged polymer melt fibers in a layer-by-layer manner [33]. Similar to conventional electrospinning, a voltage source is applied to a polymer to extract the material from a spinneret onto a collector. However, unlike electrospinning, where large distances between the spinneret and collector typically lead to whipping instabilities and unpredictable flow behaviors, MEW permits control over a stable polymer jet. The high viscosity of the polymer melt, along with a reduced spinneret-to-collector distance and the applied voltage source helps to stabilize the flow of polymer melt so that it may be predictably and directly written onto a computer-controlled collector. After controlled deposition, the rapid cooling of the polymer melt gives rise to a stable, fiber structure. Thus, the advantage of MEW over electrospinning is its ability to finely control the organization of polymer melt fibers to fabricate user-defined geometries. Moreover, highly porous, microfiber meshes can be printed via MEW at even submicron resolutions that

are not possible via traditional extrusion 3D printing [34].

HA-based hydrogels are a specific class of hydrogels that have been shown to support the chondrogenesis of MSCs, but exhibit the aforementioned limitation of significantly inferior mechanical properties when compared to native cartilage [35]. In consideration of advances in the biofabrication field, the overall aim of this study was to introduce MEW reinforcement into engineered HA hydrogels to meet desired design criteria for cartilage repair. To do this, we first screened formulations of norbornene-modified HA (NorHA) across varied crosslinking densities to identify a hydrogel formulation that would be most permissive to the formation of neocartilage. Next, MEW meshes were introduced into NorHA hydrogels to increase their initial mechanical properties and stability and the influence of MEW meshes on cartilage formation was investigated [31]. Last, composites of NorHA and MEW meshes were assessed for their integration potential with native cartilage rings. These studies collectively demonstrate that NorHA–MEW composites support the chondrogenesis of encapsulated MSCs while increasing the construct mechanical properties, both initially and over extended culture periods, suggesting that composites may improve *in vivo* integration and cartilage formation in future studies.

2. Materials and methods

2.1. Materials

Sodium HA was purchased from Lifecore Biomedical (Chaska, MN) and lithium phenyl-2,4,6-trimethylbenzoylphosphinate (LAP) was purchased from Colorado Photopolymer Solutions (Boulder, CO). Unless otherwise specified, all other reagents and materials were purchased from Sigma-Aldrich (St. Louis, MO).

2.2. Hydrogel fabrication and characterization

2.2.1. NorHA synthesis

NorHA was synthesized as previously reported [36]. Briefly, sodium HA was first converted into its tetrabutylammonium salt form (HA–TBA) and then modified with norbornene functional groups via benzotriazole-1-yl-oxy-tris-(dimethylamino)-phosphonium hexafluorophosphate (BOP) coupling. After dissolving sodium HA in distilled water, Dowex 50W × 200 resin was added to the solution in a 3:1 mass ratio. The solution was then mixed for 30 min, and Dowex resin was subsequently removed via vacuum filtration. Thereafter, the filtrate was titrated with tetrabutylammonium hydroxide solution to a pH of 7.02–7.05, frozen, and lyophilized. The resulting lyophilized HA-TBA and 5-norbornene-2-methylamine were then dissolved in anhydrous dimethyl sulfoxide (DMSO) under inert nitrogen. BOP was then added to the reaction solution via cannulation and the reaction proceeded for 2 h at room temperature. The reaction was quenched with the addition of cold distilled water and subsequently dialyzed for 5 d. Any precipitates within the crude product solution were then removed via filtration and the solution was dialyzed for an additional 3–5 d. After freezing and lyophilizing the synthesized NorHA, the extent of norbornene modification was determined via ^{1}H-NMR to be ∼22% of the disaccharide repeat units of HA (figure S1 available online at stacks.iop.org/BF/14/014106/mmedia).

2.2.2. Hydrogel fabrication

Lyophilized NorHA macromer from 2-5 wt% was dissolved in phosphate buffered saline (PBS) and LAP photoinitiator was added to a final concentration of 0.05%. DL-dithiothreitol (DTT) was subsequently added at concentrations of 0.54 mM, 2.17 mM, 5.71 mM, or 13.58 mM (to obtain compressive moduli of approximately 2, 6, 20, and 60 kPa, respectively). After all precursor materials were thoroughly mixed, hydrogels were cast into molds (diameter ∼4 mm, height ∼1 mm) and irradiated with blue light (400–500 nm, Omnicure lamp with an affixed collimator, $I = 10$ mW cm^{-2}) for 5 min.

2.2.3. Compression testing

To evaluate the compressive properties of hydrogels, samples were subjected to unconfined, uniaxial compressive testing at a constant loading rate of 0.2 N min^{-1} (Q800 DMA, TA Instruments). The compressive modulus was then quantified as the slope of the stress–strain curves between 10% and 20% strain.

2.3. Cell culture and characterization of MSC-laden constructs

2.3.1. Cell/tissue isolation and culture

Juvenile bovine knee joints were obtained (Research 87, Boylston, MA) and dissected under sterile conditions as previously described [16]. Femoral bone marrow was extracted and MSCs were isolated via plastic adherence during culture in Dulbecco's modified eagle medium (DMEM) supplemented with 10% fetal bovine serum (FBS) and 1% penicillin/streptomycin (P/S). After expansion, MSCs were washed, trypsinized (0.05%), centrifuged, and resuspended in PBS for use. NorHA macromer solution with sterile filtered LAP and DTT was prepared as described above prior to the suspension and encapsulation of MSCs (P1, 20 × 10^{6} cells ml^{-1}) with blue light exposure. Constructs (∼15 μl gel volume, ∼3 × 10^{5} cells per construct) were subsequently cultured in chondrogenic media (1% ITS+; 2.50 μg ml^{-1} amphotericin B; 1 × 10^{-3} M sodium pyruvate; 50 μg ml^{-1} ascorbic acid 2-phosphate; 40 μg ml^{-1} L-proline;

1×10^{-7} M dexamethasone; 10 ng ml^{-1} TGF-β3) for up to 56 d.

2.3.2. Cell viability

To evaluate the cytocompatibility of constructs, hydrogels were stained with calcein AM and ethidium homodimer (0, 3, 7 d) in accordance with manufacturer's instructions (Invitrogen). Cell viability was quantified via analysis of confocal images (Leica SP5) using Image J software. Viability was calculated as the number of live cells per total cells within an image ($n \geqslant 3$ hydrogels, nine images per sample).

2.3.3. Gene expression analysis and biochemical assays

Each sample was immediately placed in 1 ml ice-cold TRIzol (Invitrogen) and stored at −80 °C for later RNA isolation. Pre-processing of samples was performed by first homogenizing samples in TRIzol on ice, subsequently adding 0.2 ml of chloroform, vigorously shaking by hand for 15 s, and centrifuging for 15 min at 4 °C. RNA was then isolated by collecting and mixing the aqueous layer with equal-parts 70% ethanol via pipetting and proceeding with the RNeasy Mini kit (QIAGEN) per manufacturer's instructions; isolated RNA concentrations were then quantified (NanoDrop 1000). RNA was processed with DNase to remove any DNA impurities and then reverse-transcribed into cDNA using the High Capacity cDNA Reverse Transcription kit (Applied Biosystems). qRT-PCR reactions were performed with 10ng cDNA and Taqman probes (Life Technologies, table S1); type I collagen (Col1a1), type II collagen (Col2a1), aggrecan (ACAN), and SOX9 were selected as targets, with glyceraldehyde 3-phosphate dehydrogenase (GAPDH) used as a housekeeping gene. Relative gene expression of experimental samples was determined using the $\Delta\Delta$CT method and MSCs expanded on tissue culture plastic as the control [37].

To quantify the biochemical content of cell-laden constructs, samples were minced and digested via overnight incubation at 60 °C in solution containing papain and hyaluronidase (0.56 U ml^{-1} papain and 750–3000 U ml^{-1} hyaluronidase were dissolved in buffer containing 0.1 M sodium acetate, 10 M cysteine hydrochloric acid, and 0.05 M ethylenediaminetetraacetic acid). The dimethylmethylene blue assay was utilized to quantify the sulfated glycosaminoglycan (sGAG) content, the hydroxyproline (OHP) assay was performed to determine collagen content (Abcam Hydroxyproline Assay Kit, ab222941), and the Picogreen dsDNA assay was performed to measure total DNA content within cultured constructs [38].

2.3.4. Histology and immunohistochemistry

After culture, constructs were fixed in 10% formalin for two hours at room temperature and then washed in PBS. Samples were then dehydrated, embedded in paraffin, and sectioned (5 μm) prior to staining. sGAG deposition by embedded cells was visualized via Alcian blue staining (1%, pH 1.0, Newcomer Supply), while deposition of types I and II collagen were visualized via labeling with anti-collagen type I (COL I, mouse monoclonal anti-collagen type 1, Millipore Sigma) and anti-collagen type II (COL II, mouse monoclonal anti-collagen type II, Developmental Studies Hybridoma Bank) antibodies and staining with DAB chromogen (Millipore Sigma). To quantify staining intensity, acquired images were converted to 8-bit and then inverted [39]. For each sample section, the mean intensities for three separate and randomly selected frames were measured in Image J.

2.4. Composite fabrication and characterization

2.4.1. MEW of PCL meshes

Box-structured meshes (4 × 4 cm^2) composed of PCL (Purasorb PC 12, Corbion Inc., Gorinchem, Netherlands) were fabricated with 70 layers (1 mm height) of overlaying fibers (layered in orthogonal directions) as previously described [40]. A custom-built MEW device equipped with an electrical heating system (TR 400, HKEtec, Germany; heating temperature = 90 °C) was used to feed PCL polymer melt (feed pressure = 3 bar) through a 23 G spinneret charged by a high voltage power supply (LNC 10 000–5 pos, Heinzinger Electronic GmbH, Rosenheim, Germany). Processed PCL fibers (diameter ∼20 μm) were then collected on a computer-controlled collector plate (acceleration voltage = 5.5 kV, spinning gap = 3.3 mm, E = 1.3 kV mm^{-1}). Each mesh was fabricated with a 90° lay-down pattern and spacing between deposited fibers of 200 μm, 400 μm or 800 μm. Disc-shaped mesh constructs were obtained from printed 1 mm thick MEW meshes using a 4 mm biopsy punch.

2.4.2. Composite fabrication

To create composites combining NorHA hydrogels and PCL meshes, lyophilized NorHA macromer and meshes (4 mm diameter, 1 mm height) were first sterilized via irradiation with a germicidal lamp in a laminar flow hood. Thereafter, NorHA (matching the formulation for 2 kPa hydrogels from above) was dissolved in PBS along with sterile filtered LAP and DTT. Juvenile bovine MSCs were then trypsinized (0.05%), counted, and suspended in the macromer solution (P1, 20 × 10^6 cells ml^{-1}). This solution (100 μl) was then carefully pipetted on top of MEW meshes and allowed to fill into the interstitial spaces of the box-structured scaffolds [41]. Meshes were then flipped, so that additional macromer could be pipetted on the other side. Finally, macromer was crosslinked within the meshes via photocrosslinking with visible light irradiation as described above (∼15 μl final gel volume, ∼2.8 × 10^5 cells per construct). Since the MEW meshes incorporated within

composites account for ∼6% volume fraction, fabricated composites contained slightly fewer cells than hydrogels alone [40]; however, the overall cell density within both composites and hydrogels was conserved.

Cells and meshes within composites were visualized using CellTracker Red CMTPX dye (Invitrogen) and fluorescein isothiocyanate-bovine serum albumin (FITC-BSA, adsorbed onto PCL filaments prior to composite fabrication), respectively, and were imaged via confocal microscopy. For visualization of hydrogel within composites, FITC-BSA was encapsulated within the NorHA hydrogels during photocrosslinking. The density of cells within the top 100 μm and bottom 100 μm of composites was calculated by counting the total number of cells within randomly placed 600 $\times$ 600 μm^2 image frames ($n \geqslant 3$ hydrogels, nine images per group). Composites were cultured in chondrogenic media for up to 56 d and characterized for cell viability, gene expression, biochemical content, histology/immunohistochemistry, and biomechanics as described above and compared to hydrogels alone.

2.5. Assessment of ex vivo integration capacity

2.5.1. Fabrication of press-fit constructs in cartilage ring explants

Juvenile bovine joints were dissected in a similar fashion as previously described and osteochondral plugs were biopsied from the trochlear groove to obtain cartilage explants for *ex vivo* integration studies. After conditioning osteochondral plugs in serum-free expansion media for 1–2 d (DMEM; 1% P/S; 10 mM HEPES, 0.1 mM non-essential amino acids; 2.50 $\mu g\ ml^{-1}$ amphotericin B; 1×10^{-3} M sodium pyruvate; 50 $\mu g\ ml^{-1}$ ascorbic acid 2-phosphate; 40 $\mu g\ ml^{-1}$ L-proline) [42], cartilage rings were isolated and prepared (8 mm outer diameter, 4 mm inner diameter, 1 mm height) such that acellular composites, cell-laden composites (i.e. composites immediately after MSC encapsulation), or cell-laden composites that were pre-cultured for 28 d in chondrogenic media (cell-laden + PC, where 'PC' refers to the pre-culture period of 28 d) could be press-fit into the inner cores of cartilage rings. As a control, biopsied autologous cartilage was press-fit back into the inner cores of rings. Each of these four different press-fit constructs (i.e. autologous cartilage control, acellular, cell-laden, cell-laden + PC) were then cultured within cartilage rings in chondrogenic media for 28 d.

2.5.2. Push-out testing

The integration strength (i.e. failure stress) of press-fit constructs cultured within explanted cartilage rings was determined via push-out testing as previously described [43]. Briefly, an indenter (3.8 mm diameter) was affixed to an Instron 5848 testing device and used to push out the central core of the cartilage constructs (0.2 mm s^{-1}). The failure stress was calculated by dividing the load at failure by the lateral surface area of press-fit constructs (i.e. interfacial area).

2.5.3. MicroCT and interfacial contact area

To visualize the integration between press-fit composites (or autologous cartilage) and the cartilage rings after 28 d of culture in chondrogenic media, samples were incubated in Lugol's solution overnight at room temperature and imaged using a Scanco MicroCT 35 system (Scanco Medical, Southeastern, PA, USA; exposure: 300 ms, voltage: 55 kVp, isotropic voxel size: 6 μm). MicroCT reconstructions were then created using DragonFly software (Version 2021.1 for Windows; Object Research Systems (ORS) Inc. Montreal, Canada, 2021; software available at www.theobjects.com/dragonfly). MicroCT reconstructions were utilized to quantify the interfacial contact area between press-fit composites (or autologous cartilage) and the cartilage rings. To measure interfacial contact area, three cross-sections were first identified within every sample, such that the middle-cross section and two cross-sections one millimeter away in each orthogonal direction revealed the interface. The contact lengths at each of these cross-sections was measured, and the interfacial contact area was then calculated by assuming that the area could be approximated as the lateral surface area of an oblique cylinder.

2.6. Statistical analysis

All statistical analyses were performed using GraphPad Prism 9 software, data are reported as mean ± standard deviation, and significance for all performed analyses was determined at $p < 0.05$. Two-way ANOVAs were performed with construct formulation and culture time set as independent variables, and multiple comparisons were performed with $\alpha = 0.05$ and Tukey's honestly significant difference (HSD) post-hoc test. Comparisons between just two groups were made via student t-tests with two-tailed criteria. For comparisons between more than two groups, one-way ANOVAs were performed, with Tukey's HSD post-hoc test; Kruskal–Wallis tests were performed for non-parametric comparisons (normality assessed via Shapiro-Wilk test, $\alpha = 0.05$), with multiple comparisons performed via Dunn's multiple comparison test.

3. Results and discussion

3.1. Influence of crosslink density on cartilage formation in NorHA hydrogels

When designing hydrogels for cartilage tissue engineering, consideration must be given to the choice of material used as well as the crosslinking chemistry selected. Here, we chose HA due to its native presence in cartilage and roles in development, wound healing, and natural ECM organization and

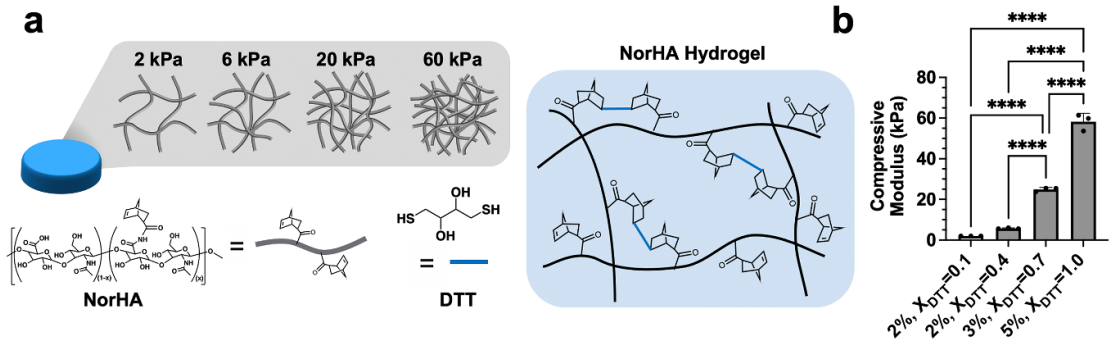

Figure 1. NorHA hydrogels with varied crosslink densities. (a) Hyaluronic acid modified with norbornene (NorHA) groups undergoes thiol-ene crosslinking in the presence of a dithiol crosslinker (DL-dithiothreitol, DTT), LAP photoinitiator, and visible light. (b) The crosslink density and compressive moduli of NorHA hydrogels are tuned (i.e. 2–60 kPa) via the polymer concentration (w/v%) and the extent of macromer crosslinking (thiol-to-norbornene ratio: X_{DTT}). $^{****}p < 0.0001$, $n = 3$.

maintenance [44]. HA possesses innate bioactivity, can be readily degraded by hyaluronidases and oxidative species, and can be easily modified with pendant functional groups for crosslinking, all of which support its use in tissue engineering applications [45]. In this work, we modified HA with norbornene groups for crosslinking via thiol-ene photocrosslinking (figure 1(a)), which enables the crosslink density to be easily modulated by the crosslinker concentration used during the step-growth crosslinking reaction [46]. Although other modifications are possible (e.g. methacrylation or MeHA), it is challenging to modify crosslinking due to the uncontrolled radical polymerization used for gelation [16]. Further, the use of NorHA not only allows for more modular control of hydrogel crosslinking, but also enables photopatterning with signaling ligands (i.e. peptides) of interest [36].

By changing both the macromer concentration and crosslinker concentration, NorHA hydrogels ranging from ∼2 to 60 kPa (figure 1(b)) were fabricated and are hereafter referred to by their approximate initial compressive moduli (i.e. 2 kPa, 6 kPa, 20 kPa, 60 kPa). Since the crosslink density of hydrogels has been previously shown to influence both encapsulated cell viability and matrix distribution by encapsulated cells [15], we first aimed to identify which hydrogel formulation best supported the viability and chondrogenesis of encapsulated MSCs. While softer, more loosely crosslinked hydrogels (i.e. 2 kPa, 6 kPa) exhibited high cell viability after 7 d of culture (∼90%), more densely crosslinked hydrogels (i.e. 20 kPa, 60 kPa) resulted in significant loss in cell viability over time (figure S2). Past fluorescent recovery after photobleaching (FRAP) studies in NorHA hydrogels suggest that the relative diffusivity of macromolecules within these networks decreases with increasing crosslink density, which may explain the observed differences in cell viability in these hydrogels [47].

To assess the ability of these hydrogel formulations to support MSC chondrogenesis and cartilage formation, cell-laden hydrogels were cultured for up to 56 d in chondrogenic media and characterized for gene expression, mechanical properties, and biochemical content. All hydrogels exhibited increased expression of aggrecan and type II collagen over time, both of which are hallmark ECM components of hyaline cartilage and suggest that embedded MSCs underwent chondrogenesis (figure 2(a)). Generally, expression of each of these genes increased the most within the first week of culture. Importantly, encapsulated MSCs also expressed SOX9, a marker of chondrogenesis [48], at early culture times, and type I collagen expression was low and decreased over culture time for 2 kPa hydrogels (figure S3).

The appearance of each hydrogel formulation noticeably changed over 56 d of culture. While more loosely crosslinked hydrogels turned opaque, suggesting the elaboration of neotissue by embedded cells, 60 kPa hydrogels remained relatively translucent (figure S4). All hydrogels also increased in compressive modulus with culture, although to varying extents based on initial crosslinking density (figure 2(b)). 2 kPa NorHA hydrogels resulted in the formation of cartilage with the highest compressive properties, reaching a compressive modulus of 102.6 ± 5.4 kPa after 28 d and 221.4 ± 33.0 kPa after 56 d. No other group reached values higher than 100 kPa, even after 56 d of culture, and the 60 kPa NorHA hydrogels barely increased in modulus with culture. These observed differences in compressive moduli were supported by the relative differences in biochemical content across each hydrogel formulation (figure 2(c)). 2 kPa hydrogels resulted in significant increases in DNA content with culture, likely due to some degree of cell proliferation, whereas the DNA content within 6 kPa hydrogels and higher were much more modest and did not significantly change throughout the duration of culture. 60 kPa hydrogels exhibited decreasing DNA content over time consistent with the observed reduction in cell viability (figure S2). With regards to biochemical content, 2 kPa hydrogels exhibited the largest increases in sGAG and collagen (COL) contents with

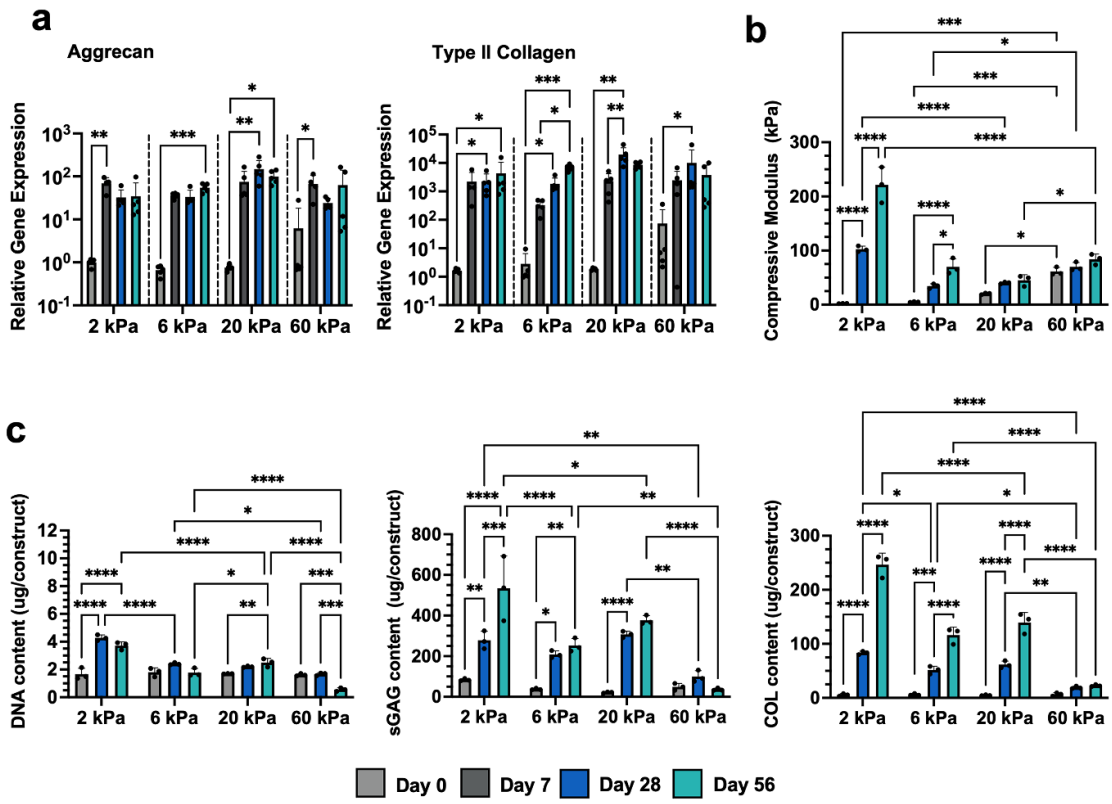

Figure 2. Influence of NorHA crosslink density on MSC chondrogenesis and neocartilage formation. Mesenchymal stromal cell (MSC)-laden hydrogels are cultured in chondrogenic media for up to 56 d and assessed for (a) chondrogenic gene expression (Aggrecan, Type II Collagen), (b) compressive moduli, and (c) biochemical content (DNA, sulfated glycosaminoglycan (sGAG), and collagen (COL)) after 0 (light gray), 7 (dark gray), 28 (blue), and 56 (teal) days of culture in chondrogenic media. $^{*}p < 0.05$, $^{**}p < 0.01$, $^{***}p < 0.001$, $^{****}p < 0.0001$, $n \geqslant 3$, individual one-way ANOVAs (20 kPa) or Kruskal–Wallis tests (2, 6, 60 kPa) performed for each hydrogel formulation for qRT-PCR data.

culture. 6 kPa and 20 kPa hydrogels similarly showed significant increases in both sGAG and COL content over the course of 56 d of culture, albeit with lower total amounts produced when compared to the 2 kPa group. Minimal changes in sGAG or COL contents were observed with the 60 kPa formulation.

These results indicate that softer NorHA hydrogels result in neocartilage with improved functional properties, and so we next aimed to elucidate the organization of nascent matrix within these hydrogels via histology for sGAG and immunohistochemistry for types I and II collagen (figures 3, S5 and S6). Alcian blue staining for sGAG revealed that 2 kPa hydrogels support increased sGAG deposition and dispersion, as indicated by significant increases in staining intensity between 28 and 56 d of culture (figure 3(a)). Moreover, 2 kPa hydrogels stained much more intensely and uniformly than the other investigated formulations, particularly at day 56. These results are consistent with past observations in MeHA hydrogels [16] and recent studies that demonstrated that the extent of nascent matrix dispersion decreases with increasing NorHA crosslink density [47]. We believe that these observed differences can be attributed to the hydrogel network being more permissive to matrix dispersion due to its increased mesh size [49], as well as the increased cell viability in less crosslinked formulations. Similar trends were observed for type II collagen staining, as 2 kPa hydrogels exhibited type II collagen that extended beyond the pericellular space of embedded cells and that was more homogenous (figure 3(b)). In contrast, dark staining localized around cells was observed in 6 kPa hydrogels after 56 d of culture, and both 20 kPa and 60 kPa hydrogels exhibited minimal type II collagen staining. Importantly, all hydrogels resulted in minimal type I collagen deposition over culture time, suggesting that hyaline-like cartilage formed within hydrogels as opposed to fibrocartilage, which is composed of more type I collagen (figure S6). Taken together, these results indicate that 2 kPa NorHA hydrogels support the formation of neocartilage *in vitro*, likely due to an increased mesh size that allows for increased matrix distribution and increased viability. The greater than 100-fold increase in compressive modulus achieved in these hydrogels over the culture period is particularly promising; however, the application of these soft hydrogels for tissue engineering is still limited by their initial mechanical properties, especially in terms of handling and stability.

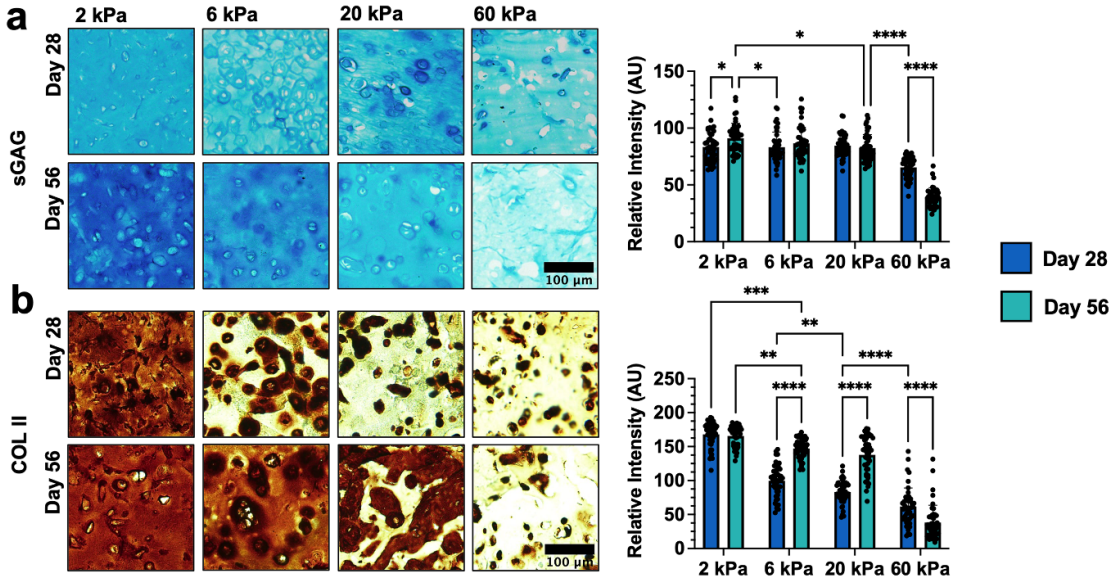

Figure 3. Influence of NorHA crosslink density on matrix production and distribution. Representative images and quantification of matrix distribution within NorHA hydrogels after 28 and 56 d of culture for (a) sGAG via Alcian blue staining or (b) type II collagen (COLII) via immunohistochemistry. $^{*}p < 0.05$, $^{**}p < 0.01$, $^{***}p < 0.001$, $^{****}p < 0.0001$, $n = 45$ images, five sections, three constructs.

3.2. Reinforcement of NorHA hydrogels with MEW meshes

To address the limitations of soft hydrogels, we reinforced the 2 kPa NorHA hydrogels with a secondary, microfiber mesh. Since MEW meshes can be readily incorporated within hydrogels to increase their compressive properties [31, 50], we first demonstrated that composites composed of NorHA hydrogels and PCL box-structured meshes could be formed by curing NorHA macromer within the interstitial spaces of MEW meshes (figure 4(a)). To permit comparisons between composites and hydrogels alone, the final dimensions of fabricated composites were matched to the initial dimensions of hydrogels alone (4 mm diameter, 1 mm thickness). The spacing between overlaying fibers within meshes was tuned between 200 μm and 800 μm to change the overall fiber density and porosity of the mesh (figure 4(b)). Interestingly, combinations of NorHA hydrogel with PCL meshes led to synergistic increases in compressive moduli, including an ~50-fold increase from the initial hydrogel modulus. The increase in mechanical properties is attributed to the ability of the hydrogel to mitigate MEW fiber buckling, which effectively increases the load-carrying capacity of MEW meshes since the PCL fibers can resist deformation in the transverse direction when loaded in compression [40]. Similarly, the presence of PCL fibers surrounding the NorHA hydrogel decreases the rate of water efflux from the hydrogel (i.e. syneresis) upon loading, further increasing the mechanical properties of the entire composite. The observed increases in compressive moduli are also consistent with similar composite systems that have leveraged MEW meshes to reinforce alternative hydrogels (i.e. gelatin, alginate, PEG, fibrin) [31, 51, 52]. The PCL fibers embedded within composites only account for ~6% of the composite's volume fraction, such that constructs may be engineered largely with a cell-laden hydrogel conducive to neotissue formation [40]. As the interfiber spacing decreases, the total fiber density within composites increases, giving rise to elevated compressive moduli (figure 4(b), S7). However, decreasing the interfiber spacing also resulted in misalignment of overlaying fibers. As a result, composites composed of meshes with 400 μm spacing were selected and employed for all subsequent studies to maximize the compressive properties of formed composites while conserving mesh alignment for optimal filling of macromer within the interstitial spaces of the mesh. All subsequent studies were also performed with 2 kPa NorHA hydrogel formulations (i.e. 2% NorHA, $X_{DTT} = 0.1$).

3.3. Neocartilage formation in MEW-reinforced NorHA hydrogels

Although the incorporation of MEW meshes within NorHA hydrogels significantly improved their compressive properties, it remained unclear how the inclusion of PCL would impact embedded MSC chondrogenesis and their ability to synthesize and distribute ECM. Thus, chondrogenesis and cartilage formation was evaluated in hydrogels alone (2 kPa NorHA) and compared to cell-laden composites containing the same hydrogel within PCL meshes (figure 5(a)). Cell viability in composites was high (92.0 ± 2.7%) after one week of culture, and homogenous filling of the hydrogel within composites was

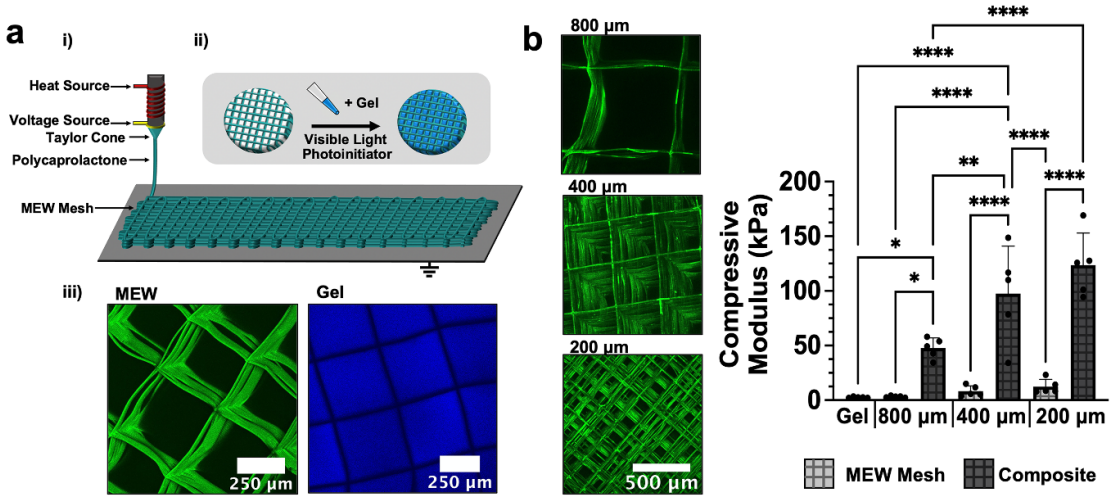

Figure 4. PCL meshes reinforce soft NorHA hydrogels. (a) (i) Schematic of the melt-electrowriting process (MEW) employed to fabricate fibrous PCL meshes. PCL is heated to form a polymer melt that can be readily extruded though a printhead with an attached voltage source to deposit PCL onto a grounded print bed. (ii) PCL meshes are then filled with NorHA macromer/crosslinker precursor (2 kPa NorHA hydrogel formulation) and exposed to visible light in the presence a photoinitiator to form composites. (iii) Images of composites containing PCL MEW meshes (green) and 2 kPa NorHA hydrogel (blue). (b) Representative images of MEW meshes of varied interfiber spacing (800 μm, 400 μm, 200 μm). Compressive moduli of NorHA hydrogel alone, PCL MEW meshes of varied interfiber spacing alone, and composites containing NorHA hydrogel infused into meshes with varied interfiber spacing. $^{*}p < 0.05$, $^{**}p < 0.01$, $^{****}p < 0.0001$, $n = 5$.

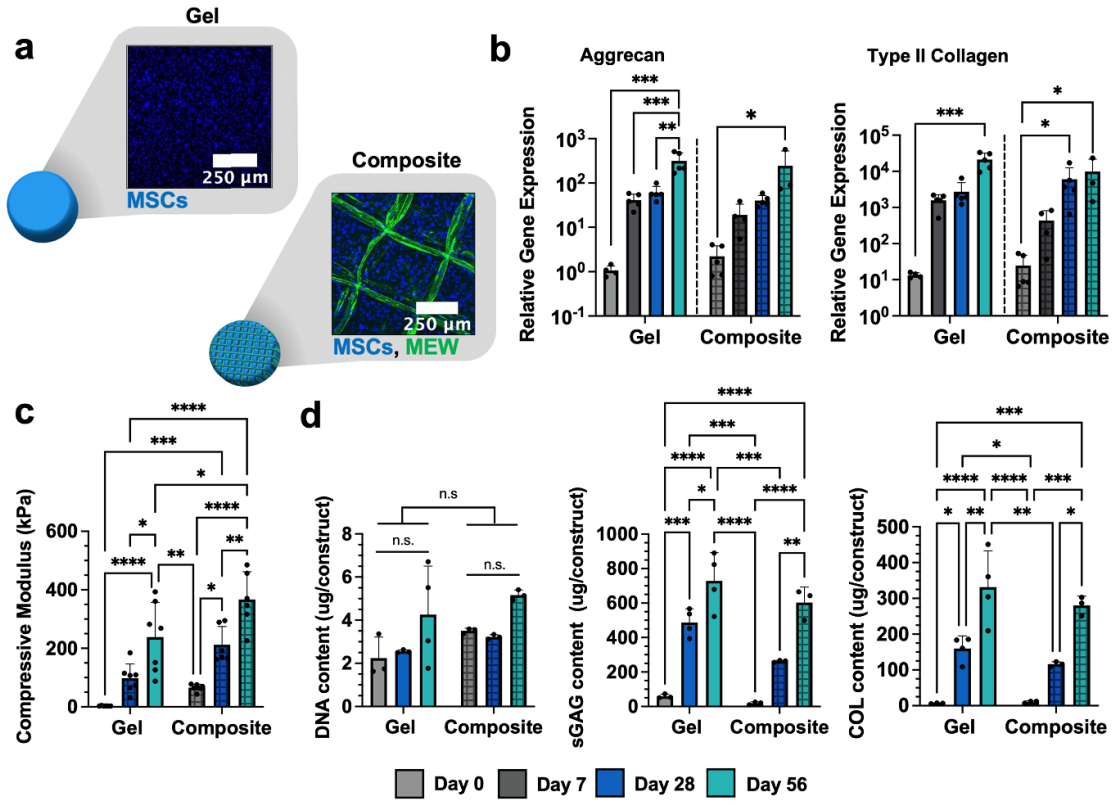

Figure 5. Influence of MEW meshes on MSC chondrogenesis and neocartilage formation. (a) Representative images of MSC-laden hydrogels and composites (2 kPa NorHA hydrogel formulation). Hydrogels and composites are cultured in chondrogenic media for up to 56 d and assessed for (b) chondrogenic gene expression (Aggrecan, Type II Collagen), (b) compressive moduli, and (c) biochemical content (DNA, sGAG, and COL) after 0 (light gray), 7 (dark gray), 28 (blue), and 56 (teal) days of culture in chondrogenic media. $^{*}p < 0.05$, $^{**}p < 0.01$, $^{***}p < 0.001$, $^{****}p < 0.0001$, n.s. = not significant, $n \geqslant 3$, individual one-way ANOVAs (Aggrecan) or Kruskal–Wallis tests (Type II Collagen) performed for each formulation for qRT-PCR data.

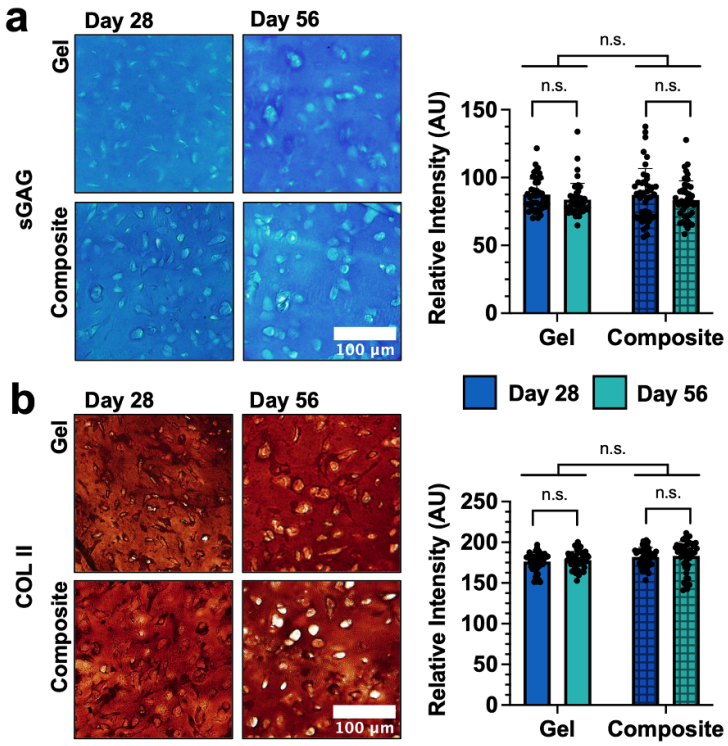

Figure 6. Influence of MEW eshes on matrix production and distribution. Representative images and quantification of matrix distribution within NorHA hydrogels and composites (2 kPa NorHA hydrogel formulation) after 28 and 56 d of culture for (a) sGAG via Alcian blue staining or (b) type II collagen (COLII) via immunohistochemistry. n.s. = not significant, $n = 45$ images, five sections, three constructs.

observed, as indicated by comparable cell densities near the top (716 ± 130 cells mm^{-2}) and bottom (638 ± 77 cells mm^{-2}) of composites (figure S8). While local heterogeneity within cell-laden hydrogels may improve neocartilage formation [53], the observation of homogenous cell densities throughout constructs ensures that matrix deposition occurs throughout the full-thickness of composites. In addition, the presence of spaces between overlaying filaments throughout the entire thickness of composites ensures that both cells and deposited ECM can permeate through the walls of the PCL box structures over time (figures 4(a) and 5(a)). As expected, MSCs exhibited significant increases in aggrecan and type II collagen expression over 56 d of culture, consistent with chondrogenesis and similar to their differentiation in hydrogels alone (figure 5(b)). Similarly, MSCs within both hydrogels alone and composites expressed SOX9 and decreasing amounts of type I collagen over culture time (figure S9).

Composites exhibited a higher compressive modulus than hydrogels alone initially and continued to increase in their mechanical properties over culture time, possessing a significantly higher modulus (367 ± 95 kPa) than hydrogels alone (239 ± 119 kPa) after 56 d of culture (figure 5(c)). Moreover, the compressive moduli of composites approached previously reported values for the Young's modulus of native articular cartilage (0.1–1.6 MPa) [54, 55]. The observed increases in mechanical properties can be attributed to the deposition of ECM by encapsulated MSCs, since acellular hydrogels and composites cultured for 56 d exhibited modest decreases in compressive properties over time due to degradation (figure S10). While all of the experimental groups exhibited increases in DNA content, no significant differences were observed across culture timepoints or between hydrogels and composites (figure 5(d)). The sGAG and COL contents for hydrogels and composites increased with culture time, with no significant differences between hydrogels or composites observed at the same culture times. Small differences in the absolute amount of sGAG or COL between composites and hydrogels alone may be attributed to the volume fraction of fibers, which slightly decreases the space available for matrix.

After 28 and 56 d of culture, dense and opaque tissue was macroscopically visible in both hydrogels alone and in composites, such that the two were indistinguishable upon qualitative observation (figure S11). The distribution of sGAG within both hydrogels and composites was comparable, with no significant differences observed in Alcian blue staining intensity (figure 6(a)). Similarly, both hydrogels and composites supported the deposition of homogenously distributed type II collagen, with no appreciable differences in staining intensity over culture time (figure 6(b)). In addition, MSCs in both hydrogels and composites deposited minimal amounts of type I collagen, consistent with a hyaline cartilage-like

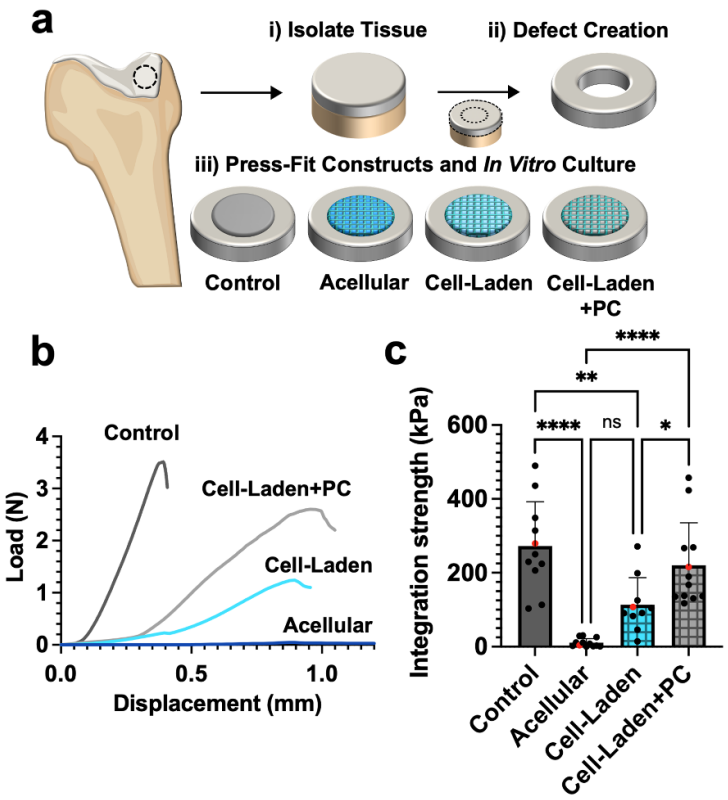

Figure 7. Integration of composites within explanted cartilage rings. (a) Schematic of integration studies. (i) Osteochondral plugs are isolated from the trochlear groove of juvenile bovine knee joints and (ii) defects are created to produce cartilage rings with an outer diameter of 8 mm and an inner diameter of 4 mm. (iii) Autologous cartilage or composites (acellular, cell-laden, and cell-laden with 28 d of chondrogenic pre-culture (+PC); 2 kPa NorHA hydrogel formulation) are then press-fit into cartilage rings, cultured for 28 d, and subjected to push-out testing. (b) Representative load-displacement curves generated during push-out testing. (c) Quantification of the integration strength of press-fit constructs with surrounding explanted tissue (red data points correspond to respective load-displacement curves in (b)). $^{*}p < 0.05$, $^{**}p < 0.01$, $^{****}p < 0.0001$, $n \geqslant 10$. Created with BioRender.com.

phenotype (figure S12). Although the staining intensity for type I collagen was significantly higher in composites at day 28 of culture, this may be attributed to the presence of additional surfaces along fibers, which may modulate gene expression and local mechanosensing of some cells [56, 57]. However, no significant difference in type I collagen staining intensity between hydrogels and composites was observed after 56 d of culture. Importantly, the observed similarities in chondrogenic gene expression, biochemical content, and matrix staining between hydrogels and composites suggests that the inclusion of PCL meshes within cell-laden NorHA hydrogels does not attenuate the ability of cells to synthesize and distribute ECM. Thus, the higher initial mechanical properties and improved handling of the composites further motivates additional exploration of their use in cartilage repair.

3.4. Integration of composites within cartilage explants

Towards translating the developed composites for the repair of focal cartilage defects, we assessed the ability of composites to integrate with explanted native cartilage *ex vivo* (figure 7(a)). After culture in chondrogenic media for 28 d, the formation of tissue resulted in changes in the opacity of press-fit cell-laden and cell-laden + PC composites (i.e. cell-laden composites that were pre-cultured for 28 d); specifically, the appearance of cell-laden + PC composites started to resemble the autologous cartilage controls (figure S13). The integration strength of press-fit constructs was then measured via push-out testing (figure S14). While acellular composites were easily displaced from the center of cartilage rings, cell-laden composites exhibited a much higher integration strength (113 ± 74 kPa; figures 7(b) and (c)). The addition of a pre-culture period and time for nascent matrix to form within composites further improved the integration strength of cell-laden + PC composites with surrounding cartilage (221 ± 115 kPa), which did not differ significantly from autologous tissue controls (272 ± 120 kPa) or previously reported integration strengths for autologous controls [43]. Uniaxial compressive testing was performed on central regions that were pushed out to confirm that culture within cartilage rings did not significantly impede cartilage formation and to compare the compressive moduli of composites with native cartilage controls (figure S15).

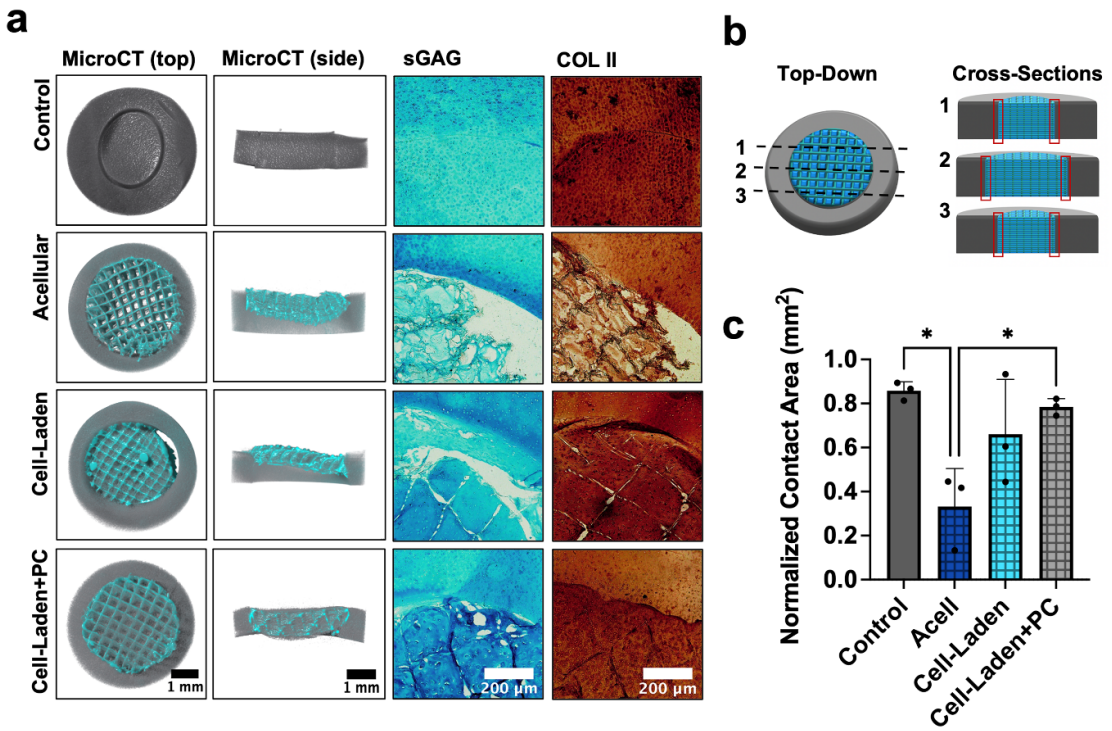

Figure 8. Characterization of composite-cartilage interfaces. (a) Representative MicroCT reconstructions, Alcian blue staining, and type II collagen (COLII) immunohistochemistry for constructs press-fit and cultured within explanted cartilage rings (2 kPa NorHA hydrogel formulation used for all composites). (b) Schematic illustrating the three cross-sections (i.e. dashed lines; midplane, and planes 1 mm from the midplane in each respective direction) analyzed to determine the interfacial contact area (indicated by red boxes). (c) Quantification of normalized contact area between press-fit constructs and native cartilage at their interfaces. $^{*}p < 0.05$, $n = 3$.

In addition to push-out testing, microCT was performed on samples to assess the interfacial contact area between press-fit composites (or autologous cartilage) and explanted cartilage rings (figures S16 and S17). The inclusion of cells within composites and the addition of a pre-culture period significantly improved composite integration with surrounding tissue (figures 8(a) and S18). The contact area between samples and cartilage rings was quantified at three different cross sections (figures 8(b) and S17) and then normalized to represent a fraction of the total possible contact area between each sample and the surrounding cartilage (figure 8(c)). While the normalized contact area was largest in control samples (0.85 ± 0.06), there were no significant differences from either of the cell-laden groups either without (0.66 ± 0.25) or with (0.78 ± 0.04) pre-culture. Notably, the normalized contact area was different between the acellular samples (0.33 ± 0.17) and both the cell-laden + PC samples and the autologous cartilage control samples. It is likely that the lack of tissue formation in acellular composites over culture time resulted in attenuated interfacial strength, as reflected by the displacement of composites and the presence of gaps between composites and native cartilage in the microCT reconstructions (figures 8(a) and S18). While these features are also pronounced in some cell-laden constructs, cell-laden + PC constructs generally showed intimate contact with the surrounding cartilage rings.

To further elucidate the interface of composites and cartilage, we stained constructs for sGAG and COLII to visualize local ECM organization (figure 8(a)). Acellular composites failed to show sGAG or COLII along the entire perimeter of the interface, consistent with our microCT quantification. While cell-laden samples similarly possessed some gaps between composites and surrounding cartilage, cell-laden samples also showed increased sGAG and COLII staining when compared to acellular samples, suggesting that the presence of nascent ECM improved overall integration. While significant changes in composite volume were not observed over culture time, the formation of GAGs within composites might increase overall composite swelling, which may further improve composite integration within cartilage rings. Of the three composite groups, cell-laden + PC constructs contained interfaces with the most continuous sGAG and COLII staining and most closely resembled autologous cartilage controls. Taken together, these results highlight the importance of hydrogel stabilization with MEW composites, as well as composite pre-culture towards developing a nascent ECM template that improves tissue integration with cartilage *ex vivo*.

4. Conclusions

In this study we demonstrated that loosely crosslinked NorHA hydrogels support MSC chondrogenesis and neocartilage formation with greater properties after culture for 56 d when compared to more densely crosslinked hydrogels. Specifically, softer NorHA hydrogels provided encapsulated MSCs with a local microenvironment more conducive to the production and distribution of ECM consistent with hyaline-like cartilage (i.e. high sGAG and COLII contents). To address the low initial mechanical properties and stability of these hydrogels, we reinforced the NorHA hydrogels with melt-electrowritten PCL scaffolds and showed that this did not inhibit MSC chondrogenesis or neocartilage formation while simultaneously providing improved mechanics and handling characteristics. Finally, we demonstrated that the chondrogenic pre-culture of NorHA–MEW composites resulted in improved tissue integration within explanted cartilage rings relative to acellular controls, informing future approaches for the fixation and maturation of cartilage implants within cartilage defects *in vivo*. Future work will implement these NorHA–MEW composites in the repair of articular cartilage defects *in vivo*.

Data availability statement

The data that support the findings of this study are available upon reasonable request from the authors.

Acknowledgments

This work was supported by the AO Foundation, the National Science Foundation (graduate research fellowship to J H G), the National Institutes of Health (R01AR077362 and T32 AR053461), the Department of Veterans Affairs (I01 RX003375 and IK6 RX003416), the University of Pennsylvania Provost Postdoctoral Research Fellowship for Academic Diversity (to C E W), and ReumaNederland (LLP-12, LLP-22, and 19-1-207). The authors would like to thank Quentin Peiffer and Cody Fell for helpful discussions, as well as Dr. Jay Patel and Dr. Claudia Loebel for assistance with MSC isolation. The authors also thank the Penn Center for Musculoskeletal Disorders (PCMD, NIH/NIAMS P30 AR069619) for support with mechanical and microCT analyses.

ORCID iDs

Claire E Witherel https://orcid.org/0000-0002-2647-0647
Miguel Castilho https://orcid.org/0000-0002-4269-5889
Robert L Mauck https://orcid.org/0000-0002-9537-603X
Jos Malda https://orcid.org/0000-0002-9241-7676
Riccardo Levato https://orcid.org/0000-0002-3795-3804
Jason A Burdick https://orcid.org/0000-0002-2006-332X

References

[1] Martín A R, Patel J M, Zlotnick H M, Carey J L and Mauck R L 2019 Emerging therapies for cartilage regeneration in currently excluded 'red knee' populations *npj Regen. Med.* **4** 12
[2] Widuchowski W, Widuchowski J and Trzaska T 2007 Articular cartilage defects: study of 25,124 knee arthroscopies *Knee* **14** 177–82
[3] Sadtler K, Singh A, Wolf M T, Wang X, Pardoll D M and Elisseeff J H 2016 Design, clinical translation and immunological response of biomaterials in regenerative medicine *Nat. Rev. Mater.* **1** 16040
[4] Heir S, Nerhus T K, Rotterud J H, Loken S, Ekeland A, Engebretsen L and Aroen A 2010 Focal cartilage defects in the knee impair quality of life as much as severe osteoarthritis: a comparison of knee injury and osteoarthritis outcome score in 4 patient categories scheduled for knee surgery *Am. J. Sports Med.* **38** 231–7
[5] Kalson N S, Gikas P D and Briggs T W R 2010 Current strategies for knee cartilage repair *Int. J. Clin. Pract.* **64** 1444–52
[6] Carey J L 2012 Fibrocartilage following microfracture is not as robust as native articular cartilage *J. Bone Jt. Surg.* **94** e80
[7] Devitt B M, Bell S W, Webster K E, Feller J A and Whitehead T S 2017 Surgical treatments of cartilage defects of the knee: systematic review of randomised controlled trials *Knee* **24** 508–17
[8] Balakrishnan B and Banerjee R 2011 Biopolymer-based hydrogels for cartilage tissue engineering *Chem. Rev.* **111** 4453–74
[9] Yang J, Shrike Zhang Y, Yue K and Khademhosseini A 2017 Cell-laden hydrogels for osteochondral and cartilage tissue engineering *Acta Biomater.* **57** 1–25
[10] Di Bella C *et al* 2018 *In situ* handheld three-dimensional bioprinting for cartilage regeneration *J. Tissue Eng. Regen. Med.* **12** 611–21
[11] O'Connell C D *et al* 2016 Development of the Biopen: a handheld device for surgical printing of adipose stem cells at a chondral wound site *Biofabrication* **8** 015019
[12] Levato R, Jungst T, Scheuring R G, Blunk T, Groll J and Malda J 2020 From shape to function: the next step in bioprinting *Adv. Mater.* **32** 1906423
[13] Lim K S *et al* 2018 Bio-resin for high resolution lithography-based biofabrication of complex cell-laden constructs *Biofabrication* **10** 034101
[14] Bernal P N, Delrot P, Loterie D, Li Y, Malda J, Moser C and Levato R 2019 Volumetric bioprinting of complex living-tissue constructs within seconds *Adv. Mater.* **31** 1904209
[15] Bryant S J and Anseth K S 2002 Hydrogel properties influence ECM production by chondrocytes photoencapsulated in poly(ethylene glycol) hydrogels *J. Biomed. Mater. Res.* **59** 63–72
[16] Erickson I E, Huang A H, Sengupta S, Kestle S, Burdick J A and Mauck R L 2009 Macromer density influences mesenchymal stem cell chondrogenesis and maturation in photocrosslinked hyaluronic acid hydrogels *Osteoarthr. Cartil.* **17** 1639–48
[17] Sridhar B V, Dailing E A, Brock J L, Stansbury J W, Randolph M A and Anseth K S 2015 A biosynthetic scaffold that facilitates chondrocyte-mediated degradation and promotes articular cartilage extracellular matrix deposition *Regen. Eng. Transl. Med.* **1** 11–21
[18] Roberts J J, Nicodemus G D, Greenwald E C and Bryant S J 2011 Degradation improves tissue formation in (un)loaded

chondrocyte-laden hydrogels *Clin. Orthop. Relat. Res.* **469** 2725–34
[19] Sahoo S, Chung C, Khetan S and Burdick J A 2008 Hydrolytically degradable hyaluronic acid hydrogels with controlled temporal structures *Biomacromolecules* **9** 1088–92
[20] Chung C, Beecham M, Mauck R L and Burdick J A 2009 The influence of degradation characteristics of hyaluronic acid hydrogels on *in vitro* neocartilage formation by mesenchymal stem cells *Biomaterials* **30** 4287–96
[21] Xu C, Dai G and Hong Y 2019 Recent advances in high-strength and elastic hydrogels for 3D printing in biomedical applications *Acta Biomater.* **95** 50–59
[22] Daly A C, Critchley S E, Rencsok E M and Kelly D J 2016 A comparison of different bioinks for 3D bioprinting of fibrocartilage and hyaline cartilage *Biofabrication* **8** 45002
[23] Xu T, Binder K W, Albanna M Z, Dice D, Zhao W, Yoo J J and Atala A 2013 Hybrid printing of mechanically and biologically improved constructs for cartilage tissue engineering applications *Biofabrication* **5** 015001
[24] Lee J S, Hong J M, Jung J W, Shim J H, Oh J H and Cho D W 2014 3D printing of composite tissue with complex shape applied to ear regeneration *Biofabrication* **6** 024103
[25] Kundu J, Shim J-H, Jang J, Kim S-W and Cho D-W 2015 An additive manufacturing-based PCL–alginate–chondrocyte bioprinted scaffold for cartilage tissue engineering *J. Tissue Eng. Regen. Med.* **9** 1286–97
[26] Critchley S, Sheehy E J, Cunniffe G, Diaz-Payno P, Carroll S F, Jeon O, Alsberg E, Brama P A J and Kelly D J 2020 3D printing of fibre-reinforced cartilaginous templates for the regeneration of osteochondral defects *Acta Biomater.* **113** 130–43
[27] Yoon Y, Kim C H, Lee J E, Yoon J, Lee N K, Kim T H and Park S H 2019 3D bioprinted complex constructs reinforced by hybrid multilayers of electrospun nanofiber sheets *Biofabrication* **11** 025015
[28] Schipani R, Scheurer S, Florentin R, Critchley S E and Kelly D J 2020 Reinforcing interpenetrating network hydrogels with 3D printed polymer networks to engineer cartilage mimetic composites *Biofabrication* **12** 035011
[29] Huang C-Y, Mow V C and Ateshian G A 2001 The role of flow-independent viscoelasticity in the biphasic tensile and compressive responses of articular cartilage *J. Biomech. Eng.* **123** 410–7
[30] Moutos F T and Guilak F 2010 Functional properties of cell-seeded three-dimensionally woven poly(ε-Caprolactone) scaffolds for cartilage tissue engineering *Tissue Eng.* A **16** 1291–301
[31] Visser J, Melchels F P W, Jeon J E, Van Bussel E M, Kimpton L S, Byrne H M, Dhert W J A, Dalton P D, Hutmacher D W and Malda J 2015 Reinforcement of hydrogels using three-dimensionally printed microfibres *Nat. Commun.* **6** 6933
[32] de Ruijter M, Ribeiro A, Dokter I, Castilho M and Malda J 2019 Simultaneous micropatterning of fibrous meshes and bioinks for the fabrication of living tissue constructs *Adv. Healthcare Mater.* **8**
[33] Robinson T M, Hutmacher D W and Dalton P D 2019 The next frontier in melt electrospinning : taming the jet *Adv. Funct. Mater.* **29** 1904664
[34] Hochleitner G, Jüngst T, Brown T D, Hahn K, Moseke C, Jakob F, Dalton P D and Groll J 2015 Additive manufacturing of scaffolds with sub-micron filaments via melt electrospinning writing *Biofabrication* **7** 035002
[35] Kim I L, Mauck R L and Burdick J A 2011 Hydrogel design for cartilage tissue engineering : a case study with hyaluronic acid *Biomaterials* **32** 8771–82
[36] Vega S L, Kwon M Y, Song K H, Wang C, Mauck R L, Han L and Burdick J A 2018 Combinatorial hydrogels with biochemical gradients for screening 3D cellular microenvironments *Nat. Commun.* **9** 614
[37] Livak K J and Schmittgen T D 2001 Analysis of relative gene expression data using real-time quantitative PCR and the 2-ΔΔCT method *Methods* **25** 402–8
[38] Kim M, Erickson I E, Choudhury M, Pleshko N and Mauck R L 2012 Transient exposure to TGF-β3 improves the functional chondrogenesis of MSC-laden hyaluronic acid hydrogels *J. Mech. Behav. Biomed. Mater.* **11** 92–101
[39] Kwon M Y, Vega S L, Gramlich W M, Kim M, Mauck R L and Burdick J A 2018 Dose and timing of N-cadherin mimetic peptides regulate MSC chondrogenesis within hydrogels *Adv. Healthcare Mater.* **7** 1701199
[40] Castilho M, Hochleitner G, Wilson W, Van Rietbergen B, Dalton P D, Groll J, Malda J and Ito K 2018 Mechanical behavior of a soft hydrogel reinforced with three-dimensional printed microfibre scaffolds *Sci. Rep.* **8** 1245
[41] Ragelle H, Tibbitt M W, Wu S Y, Castillo M A, Cheng G Z, Gangadharan S P, Anderson D G, Cima M J and Langer R 2018 Surface tension-assisted additive manufacturing *Nat. Commun.* **9** 1184
[42] Liebesny P H, Mroszczyk K, Zlotnick H, Hung H H, Frank E, Kurz B, Zanotto G, Frisbie D and Grodzinsky A J 2019 Enzyme pretreatment plus locally delivered HB-IGF-1 stimulate integrative cartilage repair *in vitro Tissue Eng.* A **25** 1191–201
[43] Erickson I E, Kestle S R, Zellars K H, Dodge G R, Burdick J A and Mauck R L 2012 Improved cartilage repair via *in vitro* pre-maturation of MSC-seeded hyaluronic acid hydrogels *Biomed. Mater.* **7** 024110
[44] Dicker K T, Gurski L A, Pradhan-Bhatt S, Witt R L, Farach-Carson M C and Jia X 2014 Hyaluronan: a simple polysaccharide with diverse biological functions *Acta Biomater.* **10** 1558–70
[45] Highley C B, Prestwich G D and Burdick J A 2016 Recent advances in hyaluronic acid hydrogels for biomedical applications *Curr. Opin. Biotechnol.* **40** 35–40
[46] Lim K S, Galarraga J H, Cui X, Lindberg G C J, Burdick J A and Woodfield T B F 2020 Fundamentals and applications of photo-cross-linking in bioprinting *Chem. Rev.* **120** 10662–94
[47] Loebel C, Kwon M Y, Wang C, Han L, Mauck R L and Burdick J A 2020 Metabolic labeling to probe the spatiotemporal accumulation of matrix at the chondrocyte–hydrogel interface *Adv. Funct. Mater.* **30** 1909802
[48] Akiyama H, Chaboissier M C, Martin J F, Schedl A and De Crombrugghe B 2002 The transcription factor Sox9 has essential roles in successive steps of the chondrocyte differentiation pathway and is required for expression of Sox5 and Sox6 *Genes Dev.* **16** 2813–28
[49] Dhote V, Skaalure S, Akalp U, Roberts J, Bryant S J and Vernerey F J 2013 On the role of hydrogel structure and degradation in controlling the transport of cell-secreted matrix molecules for engineered cartilage *J. Mech. Behav. Biomed. Mater.* **19** 61–74
[50] Castilho M, Mouser V, Chen M, Malda J and Ito K 2019 Bi-layered micro-fibre reinforced hydrogels for articular cartilage regeneration *Acta Biomater.* **95** 297–306
[51] Bas O *et al* 2017 Biofabricated soft network composites for cartilage tissue engineering *Biofabrication* **9** 025014
[52] Bas O *et al* 2018 Rational design and fabrication of multiphasic soft network composites for tissue engineering articular cartilage: a numerical model-based approach *Chem. Eng. J.* **340** 15–23
[53] Vernerey F J and Bryant S 2020 The role of percolation in hydrogel-based tissue engineering and bioprinting *Curr. Opin. Biomed. Eng.* **15** 68–74
[54] Wang C C B, Chahine N O, Hung C T and Ateshian G A 2003 Optical determination of anisotropic material properties of bovine articular cartilage in compression *J. Biomech.* **36** 339–53
[55] Töyräs J, Lyyra-Laitinen T, Niinimäki M, Lindgren R, Nieminen M T, Kiviranta I and Jurvelin J S 2001 Estimation

of the young's modulus of articular cartilage using an arthroscopic indentation instrument and ultrasonic measurement of tissue thickness *J. Biomech.* **34** 251–6
[56] Hogrebe N J, Reinhardt J W and Gooch K J 2017 Biomaterial microarchitecture: a potent regulator of individual cell behavior and multicellular organization *J. Biomed. Mater. Res.* A **105** 640–61
[57] Eichholz K F and Hoey D A 2018 Mediating human stem cell behaviour via defined fibrous architectures by melt electrospinning writing *Acta Biomater.* **75** 140–51